



# Systematic investigation of deformation behavior of tubes in a three-coil electromagnetic forming process

Shaowei Ouyang<sup>1,2</sup> · Xiaofei Xu<sup>1,2</sup> · Xiaoxiang Li<sup>1,2</sup> · Zhipeng Lai<sup>1,2</sup> · Xiaotao Han<sup>1,2</sup> · Quanliang Cao<sup>1,2</sup> · Liang Li<sup>1,2</sup>

Received: 16 June 2021 / Accepted: 11 October 2021 / Published online: 14 January 2022  
© The Author(s), under exclusive licence to Springer-Verlag London Ltd., part of Springer Nature 2021

## Abstract

The multi-coil electromagnetic forming technology developed in recent years has shown unique advantages in improving the forming ability and controllability for both tubes and sheet metals. In this work, a three-coil tube forming process is developed to improve the forming uniformity and achieve controllable forming, and the deformation behavior of the tube and corresponding deformation mechanism are systematically explored by both numerical and experimental methods. A forming process window with the voltages of the subcoils as variables is established to reveal the flexibility of the three-coil system in the shape control of deformed tubes, and to quickly evaluate the forming shape under specific discharge conditions. Meanwhile, it is demonstrated that there exists an optimum discharge voltage of the middle coil to achieve the maximum homogeneous deformation range when the discharge voltage of the upper and lower coils is fixed, while the forming height basically linearly increases with the discharge voltage of the upper and lower coils when the discharge voltage of the middle coil is fixed. Moreover, it is found that the forming uniformity of tubes can be further improved from 23.7 to 34.9 mm by increasing the distance between the upper and lower coils, and the same polarity can generate a 17.5 times stronger Lorentz force in the tube center that is preferable for higher forming efficiency. These results have certain significance for understanding the multi-coil forming process of tubes and expanding the application of electromagnetic tube forming.

**Keywords** Tube forming · Electromagnetic forming (EMF) · Lorentz force · Three-coil system · Deformation uniformity

## 1 Introduction

Electromagnetic forming (EMF) is a high-speed forming technology that shapes workpieces by Lorentz forces. It has attracted widespread attention owing to its several unique advantages in the manufacturing of aluminum alloy components, such as improved forming limit, reduced springback, and inhibited wrinkling [1]. During the EMF process, the Lorentz force is the main driving force that causes plastic deformation of the metal workpiece, so its distribution

characteristics (amplitude, pulse width, or profile) are the key to determining the final shape of the deformed workpiece [2–4].

Currently, to regulate the deformation behavior or forming shapes of workpiece, several methods have been developed by altering the Lorentz force distribution on the workpiece, which can be divided into the following four main categories: (1) by adjusting the waveform of the discharge current in the coil. For instance, Paese et al. [5] found that the Lorentz force on the sheet can be improved by optimizing the current frequency. Ouyang et al. [6] numerically and experimentally demonstrated that an attractive force can appear in the falling edge of the discharge current as its frequency decreases, which has been applied to achieve an attractive forming of aluminum alloy sheets. Cao et al. [7] proposed an EMF discharge circuit with an additional crowbar circuit, where both the oscillation and non-oscillation of the current can be achieved by changing the crowbar resistance. This method significantly increases the flexibility of EMF process and reduces the temperature rise in the coil. Du et al. [8] developed a simple and low-cost method to

✉ Quanliang Cao  
quanliangcao@hust.edu.cn

✉ Liang Li  
liangli44@mail.hust.edu.cn

<sup>1</sup> Wuhan National High Magnetic Field Center, Huazhong University of Science and Technology, Wuhan 430074, China

<sup>2</sup> State Key Laboratory of Advanced Electromagnetic Engineering and Technology, Huazhong University of Science and Technology, Wuhan 430074, China

achieve an adjustable current waveform through altering the damping coefficient of the EMF discharge circuit, and demonstrated that the Joule heating in the coil can be significantly reduced by just introducing an additional resistor, while ensuring the forming depth of workpiece unchanged; (2) by use of a new-structure coil. The flat spiral coil is the most commonly used in EMF [9–12], and it can be designed into different shapes to meet the specific forming requirements. For instance, Cui et al. [13] developed a runway coil to produce a relatively uniform Lorentz force on the alloy tensile specimens and obtained a uniformly deformed sample. Li et al. [14] proposed a sectional coil with different wire spacing to increase the forming accuracy and quality of variable-diameter tubes. Qiu et al. [15] designed a multi-layer concave coil to improve the axial inhomogeneous deformation of a long tube; (3) by introducing metallic conductive media between coil and workpiece. This method can alter the distribution of the magnetic field in space, thereby changing the Lorentz force on the workpiece. For instance, in terms of sheet forming, Kamal and Daehn [16] designed a uniform pressure actuator consisting of an inner coil and an outer conductive channel, which can provide a uniform pressure distribution on the sheet. Similarly, Wu et al. [17] proposed a uniform pressure actuator with a new structure, which consists of an inner conductive channel and an outer coil. Xu et al. [18] used a driver sheet to deform the AZ31 magnesium alloy sheet. Cao et al. [19] adopted an electromagnetically driven tool consisting of auxiliary sheet metal and a punch to deform the 5052 aluminum alloy sheet. In terms of tube forming, the use of a field shaper is the most common way to reinforce the distribution of Lorentz force. Suzuki et al. [20] found that various tube forming shapes can be achieved by different types of field shaper. Fan et al. [21] analyzed the effect of the field shaper geometry on the plastic deformation behavior of a tube, and demonstrated that the bamboo-like shape on the tube outer surface can be eliminated by the modification of a field shaper. In addition to forming, the field shaper has also been applied in EMF joining techniques [22–24]; (4) by use of a multi-coil system. This method has been proved to be a powerful tool

in controlling Lorentz force on both sheet and tube in our previous work. For instance, Lai et al. [25, 26] introduced an additional coil to promote the material flow in the flange region for deep drawing of sheet metal, and a similar method was developed for deep-cavity sheet forming by Chen et al. [27, 28] and tube forming by Zhang et al. [29]. Li et al. [30] developed a dual-coil system to enhance tube forming tube bulging through introducing a background magnetic field. Later, this method was further applied to achieve an attractive tube forming by Ouyang et al. [31].

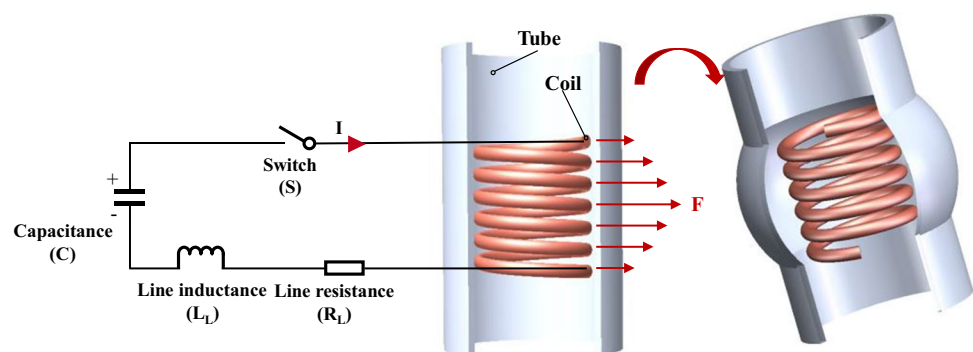
More recently, a three-coil forming system equipped with two pulsed power supplies was proposed in our previous work to alter the Lorentz force distribution on the tube [32]. It was found that the homogeneous deformation range of tubes can be increased by more than 100%, and both concave and convex profiles of tubes can be achieved. However, the work focused on verifying the feasibility of the developed system. In this work, our goal is to further systematically explore the tube deformation behavior in the EMF process with the three-coil system, and clarify how to achieve flexible control of tube shapes and obtain better forming performance. In the following sections, the design principle and implementation of the three-coil system are first introduced. Then both numerical and experimental studies based on a wider range of discharge conditions are performed to reveal the control rules for forming shapes. Meanwhile, the relationship between the forming results (forming uniformity and forming height) and the discharge voltages of the three-coil system is discussed. Finally, the effect of coil structure and coil polarity on the forming performance is studied.

## 2 Principle and method

### 2.1 Principle of the three-coil EMF

Figure 1 displays the schematic diagram of a conventional EMF system for tube forming, where the Lorentz force acting on the tube is the largest in the peripheral area of the coil center and gradually decreases toward both ends.

**Fig. 1** Schematic diagram of a conventional EMF system for tube forming



Because only one coil and a set of power supply are used, the amplitude or pulse width of the force is adjustable, but its profile characteristics on the tube is difficult to be altered, leading to a unique conical shape with poor uniformity of the tube. To solve this issue, a new EMF system consisting of three subcoils for tube forming was developed in our previous work [32]. Considering the up-and-down symmetry of the tube forming, the upper coil named Coil-1 and lower coil named Coil-3 are connected in series and activated by one power supply, while the middle coil named Coil-2 is powered individually, as schematically shown in Fig. 2. In this case, the Lorentz force distribution profile can be altered from a concave shape to a convex shape by adjusting the discharge energy of these subcoils (see Fig. 2). This indicates that by using the proposed EMF system, the forming process of the tube can be well controlled, which provides the possibility to achieve the tube bulging with high uniformity or a variety of deformed shapes.

### 2.2 Simulation model

To investigate the deformation behavior of tube utilizing a three-coil system, a simulation model created by COMSOL has been developed in this work, which contains four coupled physical models including “global ODEs and DAEs,” “magnetic fields,” “solid mechanics,” and “moving mesh” models. Similar numerical methods have been widely used for the simulation of electromagnetic forming process in our previous work [33–36]. Figure 3a shows the main structural parameters of the EMF system from a half section view, where each subcoil consists of 20 turns of conductors arranged in 5 layers. An aluminum alloy sheet (AA6061-O) is with a thickness of 2 mm, a diameter of 76 mm was used, and its physical parameters obtained from a data base of engineering material properties (<http://www.matweb.com>) are shown in Table 1. The quasi-static stress–strain ( $\sigma_{qs} - \epsilon$ ) is drawn as:

$$\sigma_{qs} = 120(\epsilon^{0.157}) \tag{1}$$

The Cowper-Symonds model is further adopted to consider the effect of the plastic strain rate ( $\epsilon_p$ ) on the dynamic stress ( $\sigma$ ):

$$\sigma = \sigma_{qs} \left[ 1 + \left( \frac{\epsilon_p}{P} \right)^m \right] \tag{2}$$

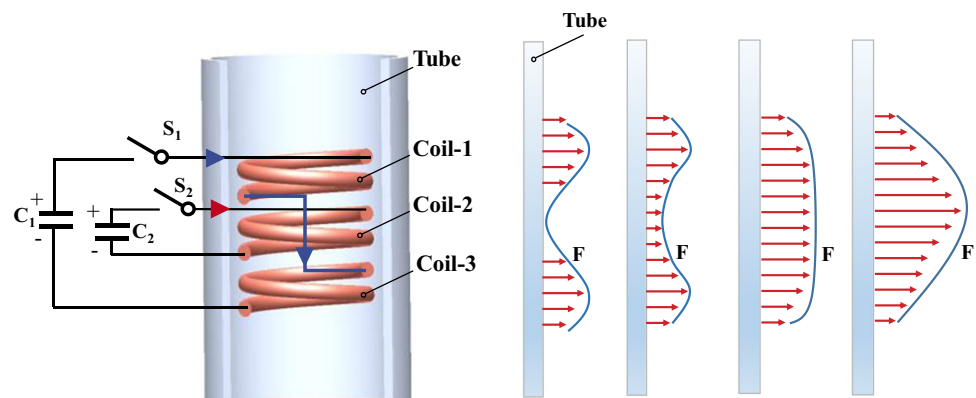
where the values of  $m$  and  $P$  are 0.25 and  $6500 \text{ s}^{-1}$ , respectively.

To improve the computational efficiency, a half model of the EMF system was built due to its symmetry, as shown in Fig. 3b. Figure 4 displays the discharge circuits for the proposed three-coil EMF system, where an additional crowbar circuit consisting of a diode and a resistor was applied. It is to be noted that the application of a crowbar circuit can reduce the temperature rise of the coil without affecting the forming efficiency [7]. The three subcoils and tube were individually treated as an equivalent circuit of an inductor and a resistor, where the Coil-1 and Coil-3 were connected in series. Two independent capacitor banks were adopted to activate the three coils, thus the discharge voltages of circuit 1 and circuit 2, denoted as  $V_1$  and  $V_2$ , could be adjusted separately. More details about the circuit parameters are provided in Table 1.

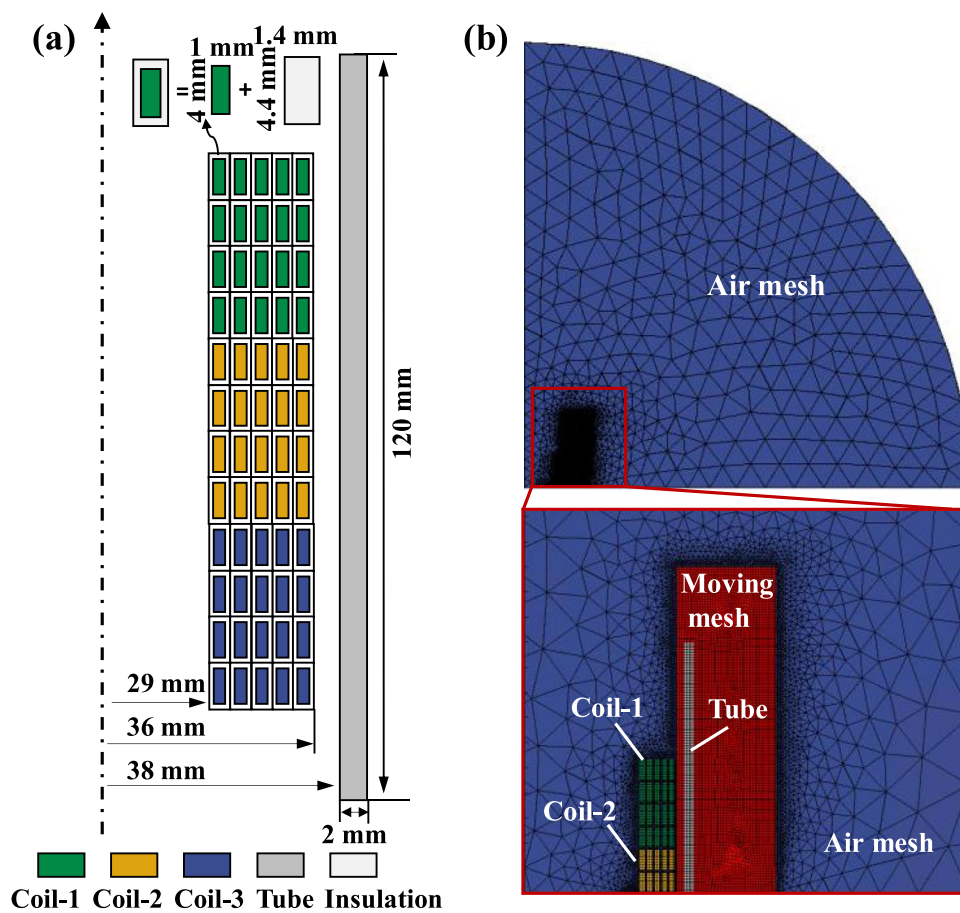
### 2.3 Experiment setup

Figure 5 shows the photo and schematic diagram of the used experiment setup, where the three subcoils were coaxially placed and reinforced with epoxy resin into a whole. The whole forming coil was pressed by epoxy boards and screws to ensure that no movement occurs during the forming process. Table 2 shows the values of discharge voltage used in experiments, where the discharge voltage for Coil-1 and Coil-3 ( $V_1$ ) was varied as 4 kV, 4.5 kV, and 5 kV, while that for Coil-2 ( $V_2$ ) was varied as 0 kV, 1 kV, 2 kV, and 3 kV. Note that the tube has broken at  $V_1 = 5 \text{ kV}$  and  $V_2 = 3 \text{ kV}$ , so an experiment with  $V_2 = 1.5 \text{ kV}$  was added in the case

**Fig. 2** Schematic diagram of the proposed three-coil system for tube forming and various types of Lorentz force distribution



**Fig. 3** The main structural parameters of the EMF system from a half section view (a) and the simulation model of the EMF system after meshing (b)



of  $V_1 = 5$  kV. In all experiments, the two discharge circuits were synchronously triggered and set to have the same polarity. Meanwhile, the discharge currents were measured by Rogowski probes, and the shape of the deformed tube was captured by a three-dimensional (3D) scanner of type PowerScan II from Vision3D company, of which the accuracy specification is no more than 0.02 mm.

### 3 Results and discussion

Before analysis, it is stipulated in this work that the forming shape of the tube with homogeneous deformation range  $L$  greater than 20 mm is flat, while that less than 20 mm is concave or convex, and the definition of  $L$  can refer to the work reported by Qiu et al. [15].

#### 3.1 Experimental validation

To validate the effectiveness of the developed system and numerical model, a series of experiments were performed with the voltage of  $V_1$  (Coil-1 and Coil-3) fixed at 5 kV. Figure 6 shows the measured and calculated discharge currents for the three-coil system and the photo of the

deformed tube in the case of  $V_2$  (Coil-2) set to 1.5 kV. The simulation results for the discharge currents agree well with the corresponding experimental data. Note that the crowbar circuits are also considered in the simulation model, and the experiment currents after the first half waveform are truncated by the thyristor switch, which is beneficial to reduce the temperature rise of the coil and has little effect on the forming process. The measured homogeneous deformation range  $L$  and forming height  $H$  were the average of the data in two mutually perpendicular directions along the tube. The value of  $H$  and  $L$  are 23.7 mm and 8.9 mm in the experiment, respectively, while those are 24.3 mm and 8.7 mm in the simulation, respectively. Further, Fig. 7 presents the photos of three typical deformed tube, and the corresponding measured and calculated outer contour of tubes, where different voltages of  $V_2$  were employed with  $V_1$  fixed at 5 kV. It can be seen that the tube is concave (homogeneous deformation range  $L < 20$  mm) under a lower  $V_2$  and gradually changes to flat (homogeneous deformation range  $L > 20$  mm) and then to convex (homogeneous deformation range  $L < 20$  mm) with increasing voltage of  $V_2$ , which basically matches with the simulation results (see Fig. 7). The various forming shapes validate the flexibility of the proposed system in adjusting

**Table 1** Simulation parameters of the three-coil EMF system

Parameter	Description	Value
A three-coil system: Coil-1 & Coil-3 power module		
$C_1$	Capacitance	320 $\mu\text{F}$
$L_1$	Line inductance	7 $\mu\text{H}$
$R_1$	Line resistance	7 $\text{m}\Omega$
$R_{d1}$	Crowbar resistance	500 $\text{m}\Omega$
$D_1$	Diode	
$S_1$	Thyristor switch	
A three-coil system: Coil-2 power module		
$C_2$	Capacitance	320 $\mu\text{F}$
$L_2$	Line inductance	48 $\mu\text{H}$
$R_2$	Line resistance	65 $\text{m}\Omega$
$R_{d2}$	Crowbar resistance	1200 $\text{m}\Omega$
$D_2$	Diode	
$S_2$	Thyristor switch	
Subcoil		
$L_{c1,2,3}$	Coil inductance	29 $\mu\text{H}$
$R_{c1,2,3}$	Coil resistance	26 $\text{m}\Omega$
Tube		
$\rho$	Density	$2.7 \times 10^3 \text{ kg/m}^3$
$\gamma$	Electrical resistivity	$2.6548 \times 10^{-8} \Omega\text{-m}$
$\nu$	Poisson's ratio	0.33
$E$	Modulus of elasticity	68.8 GPa

tube forming shapes, which is consistent with our previous work [32].

### 3.2 Plastic deformation behavior analysis

To better understand the underlying control mechanism for the variable forming shape, the dynamic deformation processes for the three typical shapes are investigated in this section, where the case with  $V_1$  fixed at 5 kV was chosen for analysis. The distribution of effective strain on the tube and deformation shape are given in Fig. 8. It can be seen that at the early stage of forming process, the main deformation of the tube in all three cases occurs on the tube sides. As the discharge voltage  $V_2$  increases, the Lorentz force loading on the middle portion of the tube increases, leading to a transition from a concave shape to a convex shape of the tube. Briefly, the introduction of the middle coil is mainly responsible for the modification of the deformation in the tube center. Figure 9 shows the evolution of the axial stress for the inner and outer surfaces at the tube center, where the forming end time was determined by the effective plastic strain. Noted that the stress oscillation after forming end time is caused by the elastic deformation and has little effect on the plastic deformation. For the concave shape, as shown in Fig. 9a, the inner and outer elements experience axial

**Fig. 4** The discharge circuits for the proposed three-coil EMF system

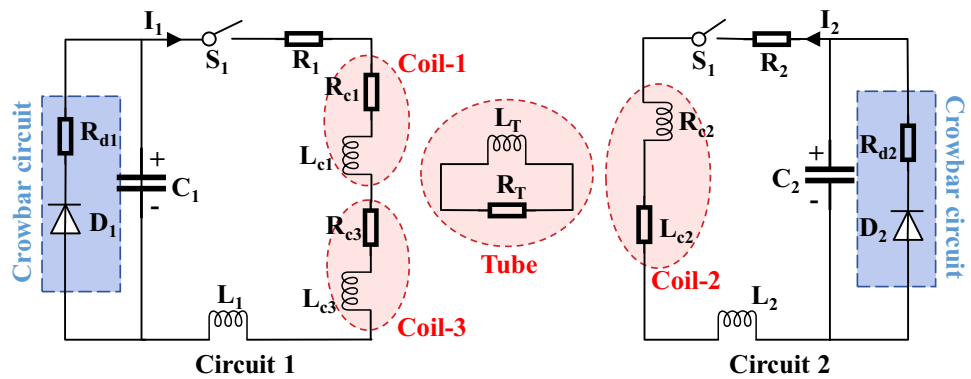


**Fig. 5** The photo and schematic diagram of the experiment setup

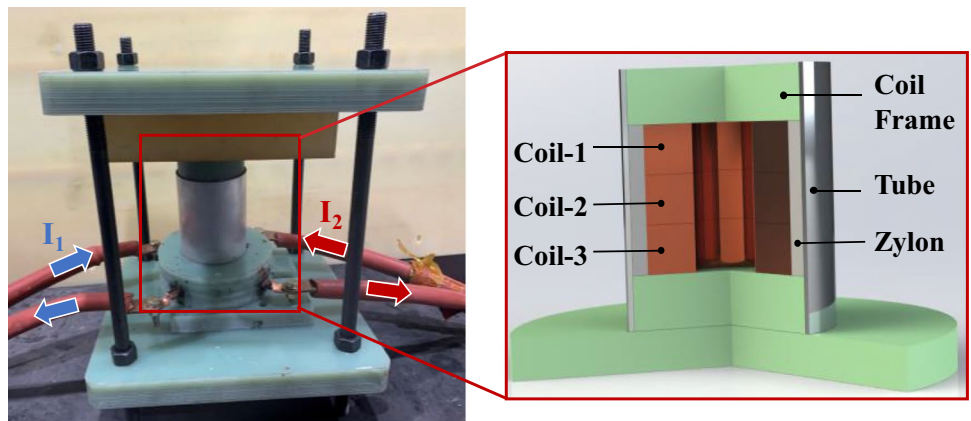


**Table 2** Discharge voltage for Coil-1,3 ( $V_1$ ) and Coil-2 ( $V_2$ ) in experiments

$V_1$ (kV)	4	4.5	5
$V_2$ (kV)	0, 1, 2, 3	0, 1, 2, 3	0, 1, 1.5, 2

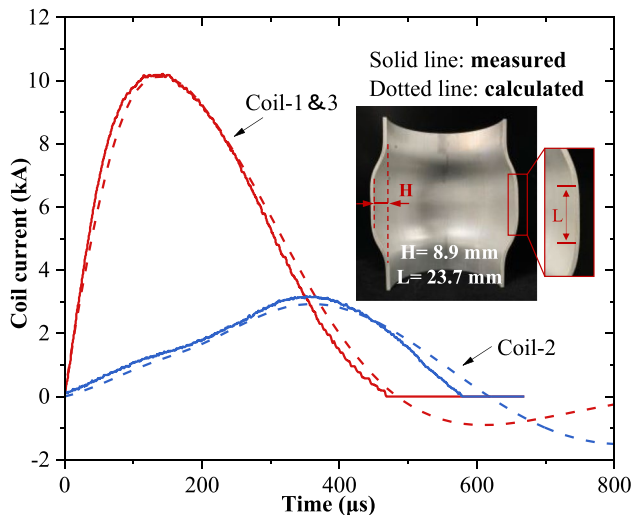


**Fig. 6** Measured and calculated discharge currents for the three-coil system and the photo of the deformed tube

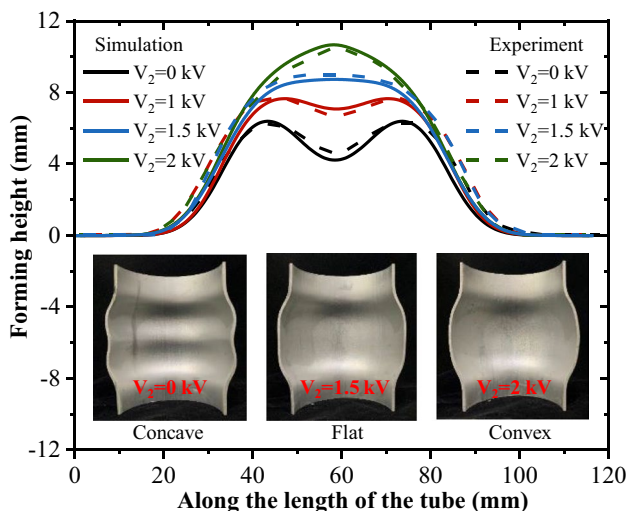


**Fig. 7** Measured and calculated results of outer contour of tubes formed by the three-coil EMF system under different discharge conditions with  $V_1$  fixed at 5 kV

tensile stress and axial compressive stress, respectively, indicating that the tube center always bends inward during the process. As a result, the tube is deformed as a concave shape. For the flat and convex shape, since the initial deformation occurs on both sides of the tube, the tube center also

undergoes axial tensile stress and axial compressive stress for the inner and outer elements, respectively. As the forming process proceeds, the axial stress of the inner and outer elements transfer to the opposite direction, as shown in Fig. 9 b and c, which indicates that the tube center starts to change from inward bending to outward bending under the action of the increasing Lorentz force on the tube center. In addition, it can be seen that a larger voltage of  $V_2$  in Fig. 9c can lead to earlier transition time. These results indicate exactly that the effective regulation of tube deformation behavior can be achieved by controlling the values of  $V_1$  and  $V_2$ .

### 3.3 Process window for shape control

To reveal the control rule for the variable forming shapes, a process window in terms of  $V_1$  and  $V_2$  based on experiments as well as extensive simulations (without considering the elongation at break) was set up, as shown in Fig. 10.

Note that the symbols marked with a circle in Fig. 10 represent the experimental data, which match well with the simulation results. The process window can be divided into three zones by taking the three typical deformation shapes as a reference. For a concave-shaped tube, it can be achieved by a combination discharge of lower  $V_1$  and  $V_2$ . As the increase of  $V_1$  or  $V_2$  to a certain extent, the tube will transform to a flat shape. In addition, the required discharge of  $V_2$  decreases with increasing  $V_1$ , and the relationship between  $V_1$  and  $V_2$  for achieving a flat tube shape can be approximately expressed as follows:

$$V_2 \approx -0.12V_1^2 + 0.44V_1 + 1.97 \quad (4 \text{ kV} \leq V_1 \leq 6.5 \text{ kV}) \tag{3}$$

The fitting curve provides a simple and effective method to distinguish the discharge voltage combinations for the three typical forming shapes, where the region for a flat shape is located near the curve, while that for a concave shape and a convex shape is located below and above the curve, respectively. As expected, as  $V_1$  or  $V_2$  further increases, the tube will transform to a convex shape. It is to be noted that the coil forming system can be treated as a kind of concave coil similar to the work reported by Qiu et al. [15] when Coil-2 is not triggered (or with a small discharge voltage). In this case, the tube can be deformed from a concave shape to a convex shape with increasing  $V_1$  in the cases of  $V_2 = 0$  kV, showing that the method using the concave coil is a case of our method. In addition, to ensure the flexibility of regulation, the discharge voltage of the upper and lower coils cannot be too large. This is because when the Lorentz force generated only by the upper and lower coils is sufficient to deform the tube into a convex shape, the use of the middle coil cannot adjust the deformation shape, as shown in the case of  $V_1 = 7$  kV in Fig. 10.

**Fig. 8** The distribution of effective strain for different deformed shapes of the tube during the forming process

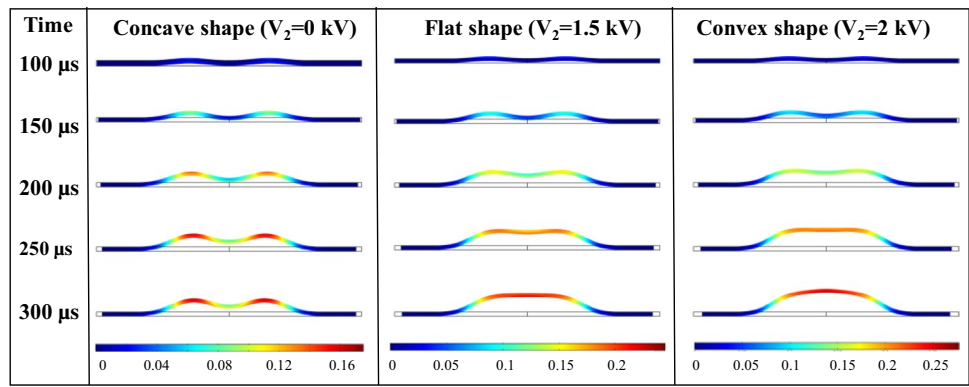
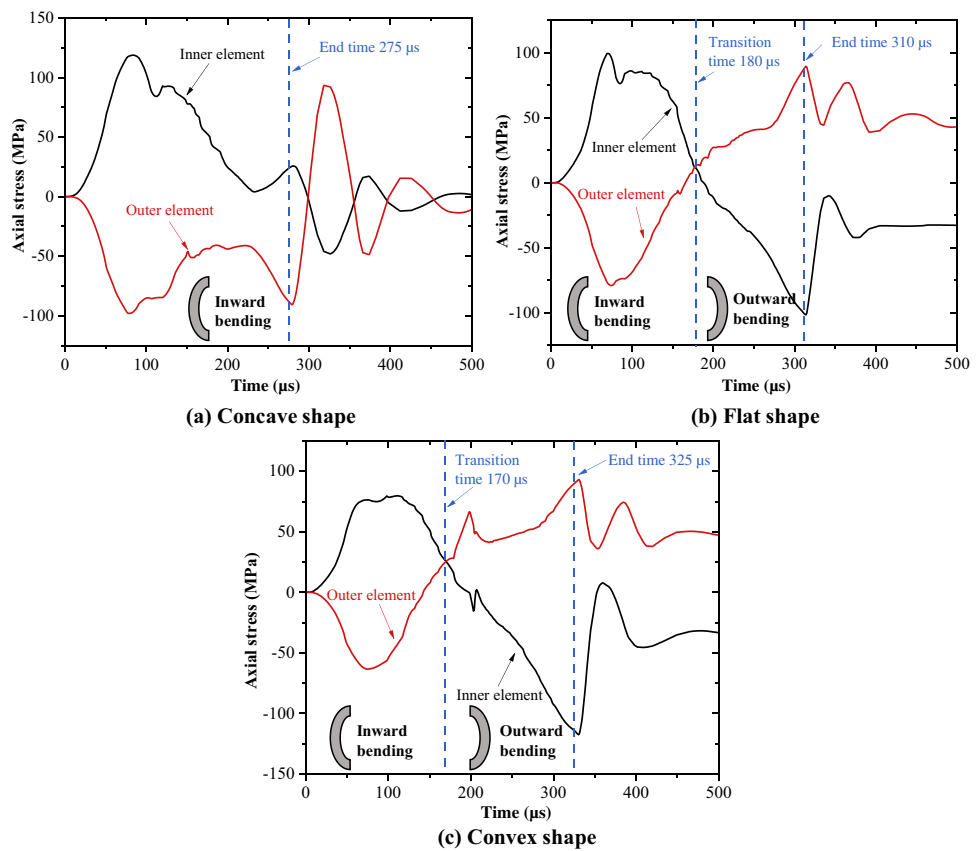


**Fig. 9** Axial stress of the inner and outer elements at the tube center varying with the time in three deformation cases. **a** The case with a concave shape. **b** The case with a flat shape. **c** The case with a convex shape



**3.4 Evaluation of forming height and uniformity**

As mentioned above, the approximate forming shape of the tube can be easily identified by the developed fitting curve. In this section, the deformation uniformity and forming height of the tube under different discharge conditions are further discussed. Figure 11 shows the simulation and experimental results for the homogeneous deformation range *L* based on the discharge conditions in Sect. 3.2, and some additional simulation results were added to enrich the data. It can be seen that there is an optimal value of *V*<sub>2</sub> for achieving the maximum homogeneous deformation range under different *V*<sub>1</sub>. It should be noted that the maximum homogeneous

deformation range in the three curves is similar according to the simulation (about 28 mm), indicating that the maximum uniformity of the deformed tube is not sensitive to the discharge energy. Further, the simulation and experimental data for the forming height are provided in Fig. 12, showing that the forming height linearly increases with *V*<sub>1</sub>, and different linear curves can be fitted with fixed *V*<sub>2</sub> based on the simulation results. Moreover, to reflect the flexibility of the proposed three-coil forming system in controlling both forming height *H* and homogeneous deformation range *L*, the distribution of *H* and *L* in terms of *V*<sub>1</sub> and *V*<sub>2</sub> is shown in Fig. 13. Obviously, the forming height *H* increases with increasing *V*<sub>1</sub> and *V*<sub>2</sub>, and the greater the *V*<sub>1</sub> is, the smaller

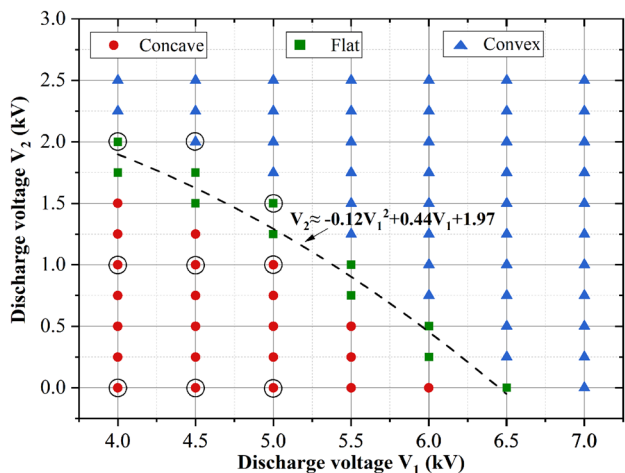


Fig. 10 Process window for forming shapes in terms of  $V_1$  and  $V_2$

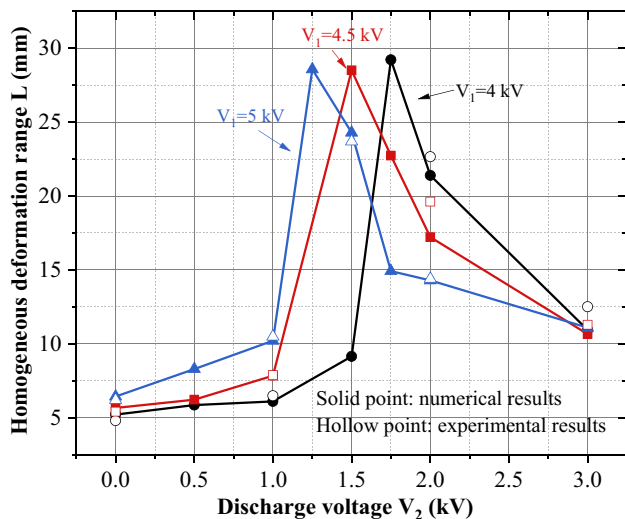


Fig. 11 Homogeneous deformation range  $L$  varying with different discharge voltage combinations

the  $V_2$  is required for the same forming height. The combinations of  $V_1$  and  $V_2$  are approximately linearly related for achieving the same forming height (see Fig. 13a), and it can be seen that there exist optimal combinations of  $V_1$  and  $V_2$  for the realization of maximum homogeneous deformation range (see Fig. 13b), and the distribution characteristic is consistent with the process window for the forming shapes. As an illustration, the contour line of  $H = 8.4$  mm in Fig. 13a was plotted in Fig. 13b, where the contour line passes through different homogeneous deformation range. This indicates that various uniformity of the tube can be realized by adjusting the discharge voltage of  $V_1$  and  $V_2$  with the forming height fixed at 8.4 mm, and the proposed three-coil system can be applied in precisely controlling the tube forming shape including uniformity and forming height.

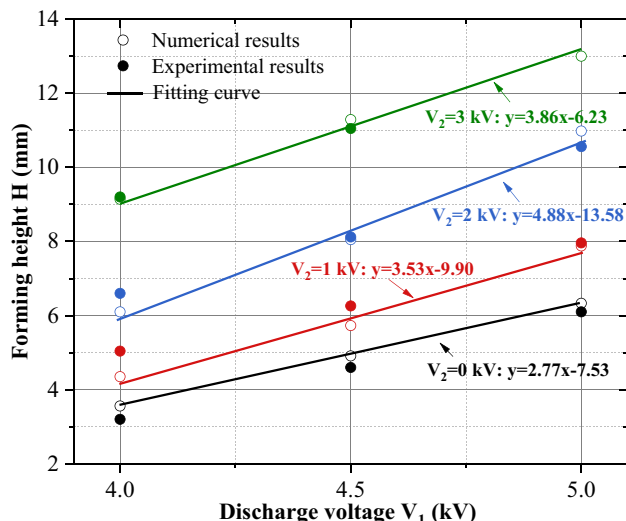


Fig. 12 Forming height  $H$  varying with different discharge voltage combinations

### 3.5 Influence of coil structure on the forming uniformity

According to Fig. 11, the maximum homogeneous deformation range  $L$  for different curves of  $V_1$  are all about 28 mm, indicating that the maximum homogeneous deformation range is independent of discharge voltage. Thus, to further improve the uniformity of the tube, the Lorentz force distribution on the tube should be improved. Figure 14 shows the dynamic forming process of one side of the tube and the maximum Lorentz force distribution (calculated by the tube fixed) on the other side of tube at the discharge combination of  $V_1 = 5$  kV and  $V_2 = 1.5$  kV. It can be seen the maximum Lorentz force is distributed as a concave shape, and the tube is concave in the early forming stage, and then gradually changes to a flat shape. It seems that the homogeneous deformation range  $L$  and concave wave distance  $d$  of Lorentz force are positively correlated, and it is possible to increase  $H$  by increasing  $d$ .

To confirm this point, the following three cases shown in Fig. 15a are considered in the simulations, where the number of turns of Coil-2 is increased from 4 to 8 with the total number of turns of these three subcoils fixed at 12. Note that the structure of case 1 represents the developed coil system in this work (see Fig. 3). Figure 15b shows the maximum Lorentz force after normalization in the three cases with a discharge combination of  $V_1 = 5$  kV and  $V_2 = 1.5$  kV, and it can be seen that the concave wave distance  $d$  increases with increasing the number of turns of Coil-2. Further, as shown in Fig. 16a, when different discharge voltages of  $V_2$  were applied with  $V_1$  fixed at 5 kV, it can be found that there is an optimal value of  $V_2$  (1.25 kV for case 1, 2.5 kV for case



**Fig. 13** The distribution of forming height **H** (a) and homogeneous deformation range **L** (b) in terms of  $V_1$  and  $V_2$

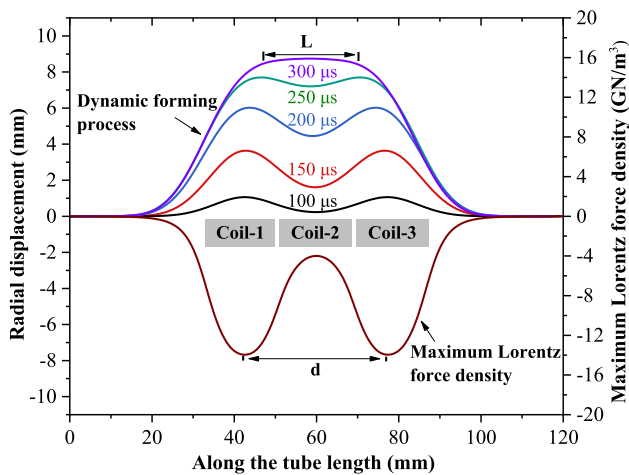
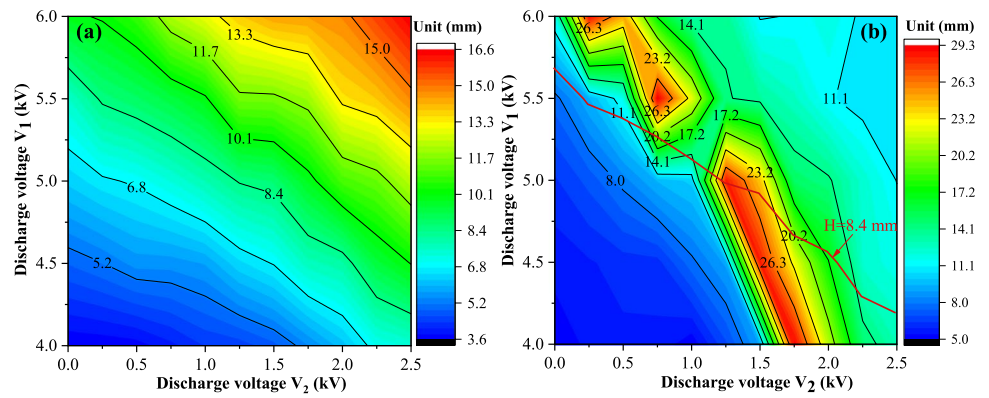


**Fig. 14** The dynamic forming process of the tube and the maximum Lorentz force distribution on the tube

2 and 3.5 kV for case 3) to achieve the maximum homogeneous deformation range **L** in all cases, and the maximum homogeneous deformation range **L** increases with increasing the number of turns of Coil-2. To verify the effectiveness of the simulation results, a new three-coil forming coil based on case 3 was developed. Figure 16b shows the photo of the deformed tubes under a discharge combination of  $V_1 = 5.5$  kV and  $V_2 = 3.7$  kV, where the homogeneous deformation range has been increased to 34.9 mm. This clearly indicates that the maximum homogeneous deformation range is directly related to the structure of subcoils, and increasing the concave wave distance **d** of Lorentz force can further improve the homogeneous deformation range **L**.

### 3.6 Influence of coil polarity on the forming process

In a multi-coil EMF process, the polarity of the current flowing in the coils could have a considerable effect on the magnetic field distribution in the workpiece, which in turn affects the forming process. It has been demonstrated

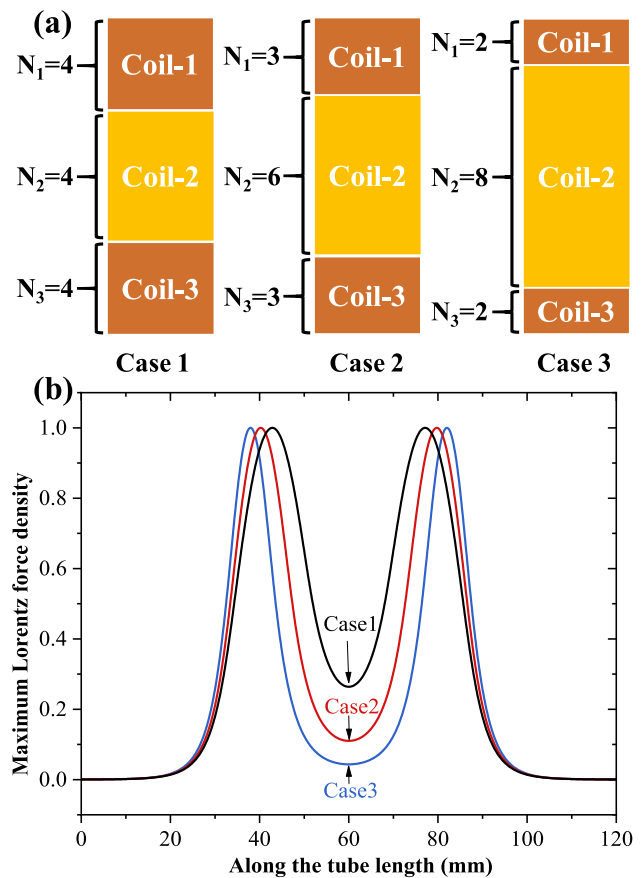
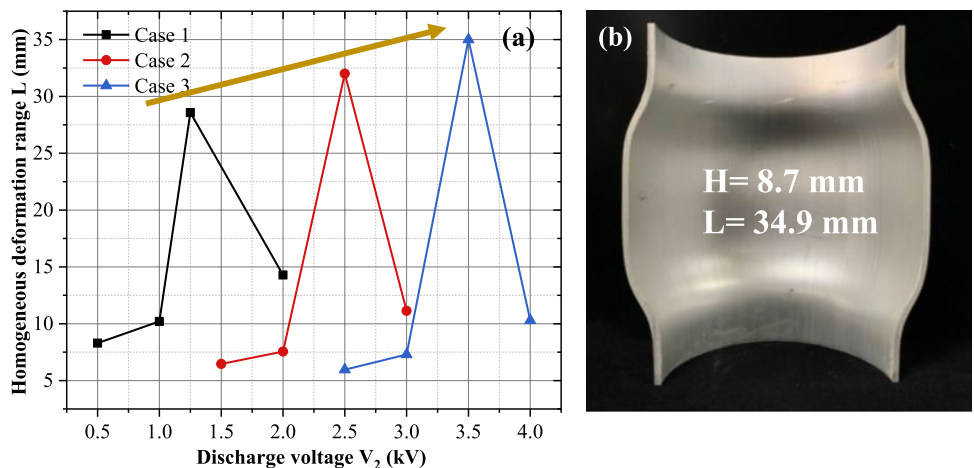


**Fig. 15** The schematic diagram of the proposed three types of coil structure (a) and the distributions of the normalized maximum Lorentz force in the three cases (b)

that the same polarity is preferable for higher energy efficiency and better forming performance in sheet metal forming process with a two-coil forming system [37]. The applicability of this rule in tube forming with a three-coil forming system should be further confirmed. Considering the up-and-down symmetry of tube forming, the direction of the current in Coil-1 and Coil-3 remains the same,

**Fig. 16** The homogeneous deformation range  $L$  varying with different discharge voltage combinations (a) and photo of the deformed tubes under a new three-coil forming system (b)



	Opposite polarity	Same polarity
Experimental		
Numerical		

**Fig. 17** Experimental and numerical results of tube shapes after deformation for the same and opposite polarities

and two cases including the same and opposite polarities of the current in Coil-2 are discussed in this section. The discharge voltages of  $V_1 = 5$  kV (Coil-1 and Coil-3) and  $V_2 = 1.5$  kV (Coil-2) were adopted for analysis. The experimental and numerical results of the deformed tubes for the same and opposite polarities are shown in Fig. 17. It can be seen that both higher homogeneous deformation range  $L$  and forming height  $H$  can be achieved in the case of the same polarity. To explain this phenomenon, the magnetic field distributions for the same and opposite polarities are shown in Fig. 18. The moment of maximum Lorentz force is chosen for analysis, where the tube is fixed without deformation. For the case of the same polarity, the magnetic field generated by Coil-2 is superimposed on that generated by Coil-1 and Coil-3, leading to a stronger magnetic field distribution near the central area of the tube

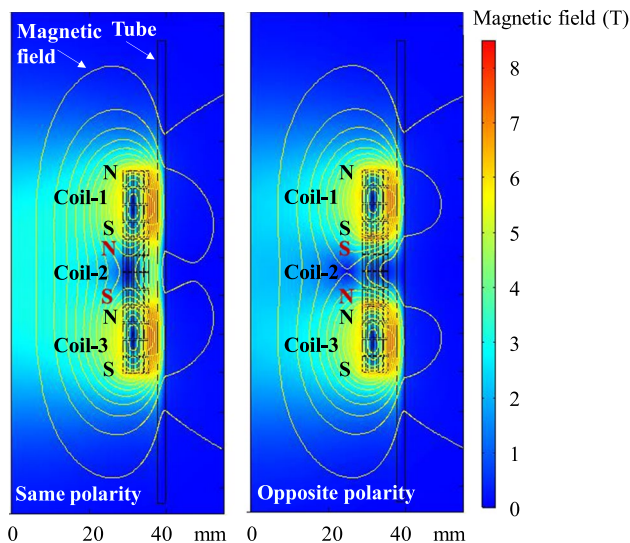
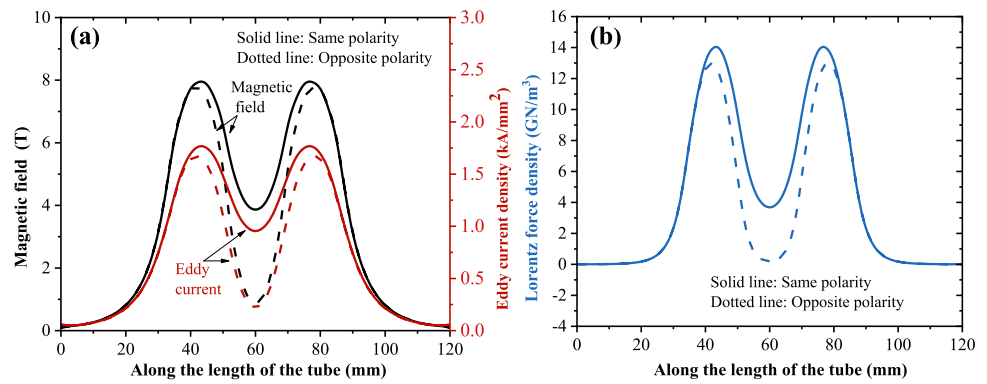


**Fig. 18** Magnetic field distributions for same and opposite polarities when the Lorentz force reaches its peak

compared to the case with opposite polarity. Figure 19a shows the magnetic field and eddy current density distribution along the tube length. It can be seen that the polarity of the Coil-2 mainly affects the magnetic field and eddy current distribution in the center area of the tube, but has minimal effect on the ends of the tube. Specifically, in the tube center area, the magnetic field and eddy current generated by the same polarity is 3.22 and 3.75 times greater than that of the opposite polarity, respectively. Thus, a 17.5 times stronger Lorentz force is induced in the tube center (see Fig. 19b) and leads to a higher forming efficiency. In addition, the three coils are mutually attractive during the forming process in the case of the same polarity, and this serves to prevent the coil frame from being dismembered by Lorentz forces.

**Fig. 19** Magnetic field and eddy current density distribution on the tube (a) and Lorentz force distribution on the tube (b)



## 4 Conclusion

This work systematically explored the application of the three-coil forming system on the controllable tube forming, and clarified the tube deformation behavior, the control mechanism, and uniformity improvement of tube forming. The main conclusions are as follows.

- (1) A process window for shape control of deformed tube was developed based on simulation data and validated by experiment data, showing that the forming shapes of the tube can be flexibly altered from convex to flat or concave by changing discharge conditions. The obtained fitting curve in the process window can be applied to quickly predict the type of forming shape in specific discharge conditions.
- (2) It was demonstrated that there exists an optimum voltage of the middle coil  $V_2$  to achieve a maximum homogeneous deformation range (about 28 mm) when the voltage of the upper and lower coils  $V_1$  is fixed, while the forming height linearly increases with the voltage of the upper and lower coils when the voltage of the middle coil is fixed.
- (3) It was found that the forming uniformity of tubes can be further improved from 23.7 to 34.9 mm by increasing the distance between the upper and lower coils, and the same polarity of subcoils can generate a 17.5 times stronger Lorentz force in the tube center, which is preferable for higher forming efficiency.

In general, this work further revealed the advantages of the three-coil system over the conventional single-coil system in the shape control of tubes. Because of this, although the three-coil forming system has higher requirements for coil manufacture and power supply, it enables EMF to be applied to occasions with specific requirements for electromagnetic force characteristics, such as the forming of high-uniformity tubes without a die and variable-diameter tubes.

**Author contribution** Shaowei Ouyang: conceptualization, investigation, methodology, writing—original draft preparation. Xiaofei Xu: investigation, writing—original draft preparation. Xiaoxiang Li: investigation, validation. Zhipeng Lai: software. Xiaotao Han: writing—review and editing. Quanliang Cao: methodology, writing—review and editing, project administration, funding acquisition. Liang Li: supervision, funding acquisition.

**Funding** This work was financed by the National Natural Science Foundation of China (51821005; 52077092) and the Young Elite Scientists Sponsorship Program by CAST (YESS, 2018QNRC001).

**Data availability** Not applicable.

## Declarations

**Ethical approval** Not applicable.

**Consent to participate** Not applicable.

**Consent to publish** All authors have read and agreed to the published version of the manuscript.

**Competing interests** The authors declare no competing interests.

## References

1. Psyk V, Risch D, Kinsey BL, Tekkaya AE, Kleiner M (2011) Electromagnetic forming—a review. *J Mater Process Technol* 211:787–829
2. Xu D, Liu X, Fang K, Fang H (2010) Calculation of electromagnetic force in electromagnetic forming process of metal sheet. *J Appl Phys* 107(12):299–310
3. Paese E, Rosa P, Geier M, Homrich RP, Rossi R (2014) An analysis of electromagnetic sheet metal forming process. *App Mech Mater* 52:9–14
4. Kleiner M, Beerwald C, Homberg W (2005) Analysis of process parameters and forming mechanisms within the electromagnetic forming process. *CIRP Ann Manuf Technol* 54(1):225–228
5. Paese E, Geier M, Homrich RP, Rossi R, Rosa P (2020) Parametric study of the design variables involved in the EMF process of sheet metal. *IEEE T Appl Supercon* 30(4):1–1
6. Ouyang S, Li C, Du L, Li X, Lai Z, Peng T, Han X, Cao Q, Li L (2020) Electromagnetic forming of aluminum alloy sheet metal utilizing a low-frequency discharge: a new method for attractive forming. *J Mater Process Technol* 291:117001

7. Cao Q, Han X, Lai Z, Xiong Q, Zhang X, Chen Q, Xiao H, Li L (2015) Analysis and reduction of coil temperature rise in electromagnetic forming. *J Mater Process Technol* 225:185–194
8. Du L, Xia L, Li X, Qiu L, Lai Z, Chen Q, Cao Q, Han X, Li L (2021) Adjustable current waveform via altering the damping coefficient: a new way to reduce Joule heating in electromagnetic forming coils. *J Mater Process Technol* 293:117086
9. Liu N, Lai Z, Cao Q, Han X, Huang Y, Li X, Chen M, Li L (2019) Effects of air on metallic sheet deformation by electromagnetic forming. *Int J Adv Manuf Technol* 103:311–324
10. Liu N, Lai Z, Cao Q, Huang Y, Chen M, Li C, Han X, Li L (2020) Effects of the inner/outer diameters of flat spiral coils on electromagnetic sheet metal formation. *Int J Adv Manuf Technol* 109:1541–1551
11. Lai Z, Han X, Cao Q, Li Q, Zhou Z, Liang L (2013) The electromagnetic flanging of a large-scale sheet workpiece. *IEEE Trans Appl Supercon* 24(3):1–5
12. Seth M, Vohnout VJ, Daehn GS (2005) Formability of steel sheet in high velocity impact. *J Mater Process Technol* 168(3):390–400
13. Cui X, Zhang Z, Yu H, Cheng Y, Xiao X (2019) Dynamic uniform deformation for electromagnetic uniaxial tension. *Metals* 9:425
14. Li J, Qiu W, Huang L, Su H, Tao H, Li P (2018) Gradient electromagnetic forming (GEMF): a new forming approach for variable-diameter tubes by use of sectional coil. *Int J Mach Tools Manuf* 135:65–77
15. Qiu L, Li Y, Yu Y, Abu-Siada A, Xiong Q, Li X, Li L, Su P, Cao Q (2019) Electromagnetic force distribution and deformation homogeneity of electromagnetic tube expansion with a new concave coil structure. *IEEE Access* 7:117107–117114
16. Kamal M, Daehn GS (2007) A uniform pressure electromagnetic actuator for forming flat sheets. *J Manuf Sci Eng* 129:369–379
17. Wu Z, Cao Q, Fu J, Li Z, Wan Y, Chen Q, Li L, Han X (2020) An inner-field uniform pressure actuator with high performance and its application to titanium bipolar plate forming. *Int J Mach Tools Manuf* 155:103570
18. Xu J, Xie X, Wen Z, Cui J, Zhang X, Zhu D, Liu Y (2019) Deformation behaviour of AZ31 magnesium alloy sheet hybrid actuating with Al driver sheet and temperature in magnetic pulse forming. *J Manuf Process* 37:402–412
19. Cao Q, Du L, Li Z, Li L, Li Z, Li X, Lai Z, Chen M, Chen Q, Xu S, Han X (2019) Investigation of the Lorentz-force-driven sheet metal stamping process for cylindrical cup forming. *J Mater Process Technol* 271:532–541
20. Suzuki H, Murata M, Negishi H (1987) The effect of a field shaper in electromagnetic tube bulging. *J Mech Work Technol* 2:229–240
21. Fan Z, Yu H, Li C (2016) Plastic deformation behavior of bi-metal tubes during magnetic pulse cladding: FE analysis and experiments. *J Mater Process Technol* 229:230–243
22. Geier M, Paese E, Rossi R, Rosa P, Homrich RP (2020) Experimental analysis of the interference-fit joining of aluminum tubes by electromagnetic forming. *IEEE Trans Appl Supercon* 30(4):1–1
23. Lueg-Althoff J, Bellmann J, Hahn M, Schulze S, Beyer E (2019) Joining dissimilar thin-walled tubes by magnetic pulse welding. *J Mater Process Technol* 279:116562
24. Rajak AK, Kumar R, Basumatary H, Kore SD (2018) Numerical and experimental study on effect of different types of field-shaper on electromagnetic terminal-wire crimping process. *Int J Precis Eng Manuf* 19(3):453–459
25. Lai Z, Cao Q, Zhang B, Han X, Zhou Z, Xiong Q, Zhang X, Chen Q, Li L (2015) Radial Lorentz force augmented deep drawing for large drawing ratio using a novel dual-coil electromagnetic forming system. *J Mater Process Technol* 222:13–20
26. Lai Z, Cao Q, Han X, Huang Y, Deng F, Chen Q, Li L (2017) Investigation on plastic deformation behavior of sheet workpiece during radial Lorentz force augmented deep drawing process. *J Mater Process Technol* 245:193–206
27. Chen M, Lai Z, Cao Q, Han X, Liu N, Li X, Huang Y, Li L (2019) Investigation on deformation control of sheet metal in radial Lorentz force augmented deep drawing. *Int J Adv Manuf Technol* 105:2369–2381
28. Chen M, Lai Z, Cao Q, Han X, Wang C, Liu N, Li L (2020) Improvement on formability and forming accuracy in electromagnetic forming of deep-cavity sheet metal part using a dual-coil system. *J Manuf Process* 57:209–221
29. Zhang X, Cao Q, Han X, Chen Q, Lai Z, Xiong Q, Deng FX, Li L (2016) Application of triple-coil system for improving deformation depth of tube in electromagnetic forming. *IEEE Trans Appl Supercon* 26(4):1–4
30. Li X, Cao Q, Lai Z, Ouyang S, Liu N, Li M, Han X, Li L (2020) Bulging behavior of metallic tubes during the electromagnetic forming process in the presence of a background magnetic field. *J Mater Process Technol* 276:116411
31. Ouyang S, Li X, Li C, Du L, Peng T, Han X, Li L, Lai Z, Cao Q (2020) Investigation of the electromagnetic attractive forming utilizing a dual-coil system for tube bulging. *J Manuf Process* 49:102–115
32. Ouyang S, Wang C, Li C, Li X, Lai Z, Peng T, Han X, Cao Q, Li L (2021) Improving the uniformity and controllability of tube deformation via a three-coil forming system. *Int J Adv Manuf Technol* 114:1533–1544
33. Cao Q, Li L, Lai Z, Zhou Z, Xiong Q, Zhang X, Han X (2014) Dynamic analysis of electromagnetic sheet metal forming process using finite element method. *Int J Adv Manuf Technol* 74:361–368
34. Cao Q, Li Z, Lai Z, Li Z, Han X, Li L (2019) Analysis of the effect of an electrically conductive die on electromagnetic sheet metal forming process using the finite element-circuit coupled method. *Int J Adv Manuf Technol* 101:549–563
35. Du L, Li X, Xia L, Zhang X, Lai Z, Han X, Li L, Cao Q (2021) Numerical and experimental verification of an iterative coupling method for analyzing the Lorentz-force-driven sheet metal stamping process. *Int J Adv Manuf Technol* 1–13
36. Cao Q, Xia L, Li X, Du L, Lai Z, Han X, Li L (2021) The importance of coil conductivity and eddy current effects in the analysis of electromagnetic forming process. *High Voltage*. <https://doi.org/10.1049/hve2.12109>
37. Lai Z, Cao Q, Chen M, Liu N, Li X, Huang Y, Han X, Li L (2019) The effect of coil polarity on electromagnetic forming using a multi-coil system. *Int J Adv Manuf Technol* 103:1555–1566

**Publisher's Note** Springer Nature remains neutral with regard to jurisdictional claims in published maps and institutional affiliations.